Stability analysis of electroconvection with a solid-liquid interface via the lattice Boltzmann method

Kang Luo,[1,2] Jian Wu,[1,2] Alberto T. Pérez,[3] Hong-Liang Yi,[1,2,*] and He-Ping Tan[1,2]

[1]*School of Energy Science and Engineering, Harbin Institute of Technology, Harbin 150001, People's Republic of China*

[2]*Key Laboratory of Aerospace Thermophysics, Harbin Institute of Technology, Harbin 150001, People's Republic of China*

[3]*Departamento de Electrónica y Electromagnetismo, Facultad de Física, Universidad de Sevilla, Avenida Reina Mercedes s/n 41012 Sevilla, Spain*

(Received 28 March 2019; published 28 August 2019)

In this paper, the electroconvective flow induced by the unipolar charge injection is extended from single-phase dielectric liquid to the solid-liquid interaction problem. The physical model with fully coupled mathematical equations is built in the liquid, solid, and interface for both the Ohmic and non-Ohmic solid models. An improved lattice Boltzmann model (LBM) is developed with three lattice Boltzmann equations for Poisson's equation, charge conservation equation, and Navier-Stokes equations, respectively. Our codes are first validated by the analytical solutions at the hydrostatic state. It is found that the LBM can well reproduce the discontinuous changes of electrical field and charge density at the interface and agrees well with the analytical results. Then, simulations are conducted under different governing parameters and interface position f_l. Results show that the bifurcation of electroconvection in the presence of the solid-liquid interface is still of subcritical type, but both the linear and finite amplitude stability criteria increase due to a voltage drop happening at the solid phase. Besides, the stability criterion expressed by the electrical Rayleigh number T_c increases as the permittivity ratios ε_r and the mobility ratios K_r increase, but T_c decreases with the increasing of dimensionless electric conductivity S and the interface position f_l.

DOI: 10.1103/PhysRevFluids.4.083702

I. INTRODUCTION

The flow motion driven by the Coulomb force exerted by the electric field on free-space charges are fundamental problems in electrohydrodynamics (EHD) [1]. Such flow plays an important role in a wide range of applications in industrial processes, such as EHD pumps, EHD turbulent mixer, electrostatic precipitators, flow control, and heat-transfer enhancement [2–7]. Extensive studies have been devoted to this problem from the aspects of stability analysis [8–10], experimental studies [7,11–13], and numerical simulations [14–18]. However, most of these studies are limited to single-phase dielectric liquids. Actually the EHD-based techniques show even more promising applications with multiphase systems containing a solid-liquid interface [19]. Some representative cases include EHD enhancement solid-liquid phase change [20,21], and dielectric barrier injectors [5]. The common fundamental of these applications is the electroconvection problem in the presence of a solid-liquid interface.

*yihongliang@hit.edu.cn

When compared to the previously established single-phase liquid model, additional equations should be added at the interface to keep the continuity of electric current at the two-phase EHD system. In addition, special treatments are required at the phase interface where extra electric forces and surface charge accumulation may exist. [22,23]. In some preliminary works, different kinds of interfaces in EHD systems have been considered, such as air-liquid, air-solid, and liquid-liquid interfaces. Chicón *et al.* [22,23] conducted a linear stability analysis of an interface between air and a low-conducting liquid. They reported both the volumetric instability and the rose-window instability in the presence of an air-liquid interface. Li *et al.* [24] investigated the surface charges and an electrical tangential shear stress at the liquid-liquid interface owing to the different conductivities of the two fluids. Jayaraman and Shyy [25] studied the electrical discharge induced by surface accumulated charge at the air-solid interface between two electrodes separated by an insulating solid dielectric barrier.

However, a mathematic model has not been well established for conjugate charge transport at the solid-liquid interface, which greatly limited the burgeoning applications of the applications of EHD on the fluid-structure interaction and the solid-liquid phase-change heat-transfer problems. Louste *et al.* [5] experimentally tested a dielectric solid barrier immersed in silicon oil to observe the charge injection induced wall jet with vortices. They reported the combination of double layer and charge injection should expect to develop reversible actuators which may be very interesting for flow control applications. Quite recently, Nakhla *et al.* [20,21] conducted two experimental studies about the EHD enhancement solid-liquid phase-change process by testing paraffin wax and Octadecane; they reported a melting time saving of 40% can be achieved under DC electric field. More complete mathematical models as well as numerical schemes are encouraged to gain fundamental insights into these interesting phenomena.

When using conventional computational fluid-dynamics methods such as finite-difference, finite-volume, and finite-element methods for conjugate transport problems, a popular approach to implement the conjugate interface condition is to apply iterative methods in which a Dirichlet interface condition is imposed for one phase and a Neumann interface condition for the other [26]. Equations in each phase are separately solved and the continuity condition at the interface is gradually satisfied through iterations. However, when extending to the conjugate charge transport problems, these iterative methods may become difficult to implement. Due to the nonlinear coupling between the Poisson equation and the Nernst-Planck equations, the iterative approach requires a considerable amount of computational effort. Moreover, the iterative methods are hard to capture the discontinuities in the distributions of electric field and charge density. Therefore, our main purpose of this work is to build a simple but efficient numerical algorithm in the framework of the lattice Boltzmann method (LBM). For each field, we plan to use only one lattice Boltzmann equation (LBE) for the whole computational domain without any special treatment at the solid-liquid interface.

During the last three decades, the LBM has experienced rapid development and has become an well-established numerical scheme for both simple and complex flows [27–29]. Owing to its kinetic particulate nature, the LBM has some attractive advantages such as simplicity of calculation, easy programming and intrinsic parallelism [30]. Only in recent years the LBM has been introduced into EHD problems, such as electrokinetic flows [31], electroconvection [32], and electrothermoconvection [33–36]. Specifically, for the model problem of electroconvection induced by unipolar injection, our LBM accurately reproduced the subcritical bifurcation of the linear instability and finite-amplitude bifurcation behaviors. However, no existing LBM models can be developed for EHD problems with a solid-liquid interface. The first work that explicitly addressed the solid-liquid interface condition in the LBM was conducted by Wang *et al.* [37] in simulating the conjugate heat transfer. They proposed a simple "half-lattice division" treatment scheme without special treatment, and the continuity condition at the interface can be automatically satisfied for steady cases. This half-lattice division scheme has been rapidly extended to the conjugate heat- and mass-transfer problems under the framework of LBM [38,39]. In this paper, the idea of half-lattice division is adopted and cooperates with the well-designed LBEs for Poisson equation and Nernst-Planck equations.

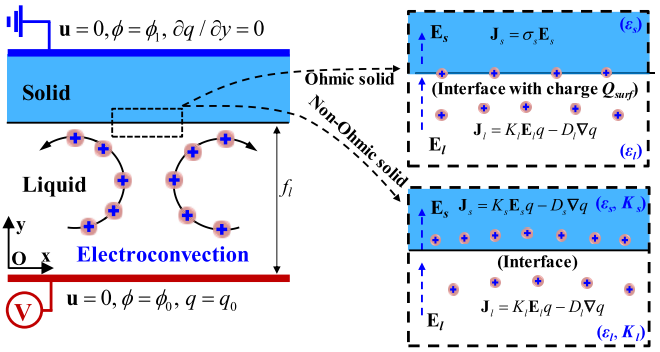

FIG. 1. Schematic diagram of electroconvective flows with solid-liquid interface. Interface zoom in sketch maps for both the Ohmic and non-Ohmic cases are presented on the right side.

In this work, we study the electroconvection between two electrodes separated by a low electric conductivity solid. To simplify the problem, we divide the solid barrier into two kinds, namely, the "Ohmic solid" and the "non-Ohmic solid" distinguished by the charge-transport mechanism in the solid region. A LBM model is developed for this EHD fluid-solid interaction problem. Three consistent lattice Boltzmann equations are built to calculate the fluid velocity, electric potential, and charge-density distributions respectively. The remainder of the present paper is organized as follows. In the next section, the physical model with the mathematical equations and the lattice Boltzmann model are presented. In Sec. III, code validation and numerical results are presented. Finally, the conclusions are drawn in the last section.

II. PHYSICAL MODELS AND MATHEMATIC FORMULATIONS

As shown in Fig. 1, the configuration consists of two planar electrodes of length L placed horizontally at a distance of H from each other. The aspect ratio of the configuration is set to be the critical wavelength ($L/H = 1.228$) [8]. A direct current (DC) electric field is established by setting the two electrodes with constant but different electric potentials. The high-voltage electrode is exposed to a dielectric liquid while the grounded electrode is encapsulated by a solid substance. Free charges are first injected from the high-voltage electrode and transport in the liquid with a drift velocity proportional to the electric field, then across the solid-liquid interface by different mechanisms depending on the physical properties of the solid substance. To simply the problem, the injected charge density at the emitter electrode q_0 is assumed to be constant and uniform (*autonomous* and *homogeneous*). The system possesses a linear instability characteristic, that is, when the driving parameter, electric Rayleigh number T, exceeds its linear stability criteria T_c, convection will arise in the liquid region under the effect of the Coulomb force and in turn affects the transport of free charges.

A. Equations in the liquid region

The fluid is assumed to be incompressible, Newtonian, and linear isotropic, and only the Coulomb force $\mathbf{F} = q\mathbf{E}$ acts on the fluid. The classical EHD governing equations include the Navier-Stokes equations and a reduced set of Maxwell's equations in the electroquasistatics limit. Basic macroscopic EHD equations in the liquid region can be expressed as [1]

$$\nabla \cdot (\varepsilon_l \nabla \phi) = -q_l, \tag{1}$$

$$\mathbf{E}_l = -\nabla \phi, \tag{2}$$

$$\frac{\partial q_l}{\partial t} + \nabla \cdot \mathbf{J} = 0, \quad \mathbf{J} = (K_l \mathbf{E}_l + \mathbf{u}) q_l - D_l \nabla q_l, \tag{3}$$

$$\frac{\partial \rho}{\partial t} + \nabla \cdot (\rho \mathbf{u}) = 0, \tag{4}$$

$$\frac{\partial (\rho \mathbf{u})}{\partial t} + \nabla \cdot (\rho \mathbf{u}\mathbf{u}) = -\nabla \hat{p} + \nabla \cdot (\mu \nabla \mathbf{u}) + q_l \mathbf{E}_l. \tag{5}$$

where $\mathbf{u} = [u, v]$ is the fluid velocity; $\mathbf{E} = [E_x, E_y]$ is the electric field; $\mathbf{J}$ is the current density; ϕ, q, ε, K, D, ρ, μ, and ν are the electric potential, charge density, permittivity, ion mobility, charge-diffusion coefficient, fluid density, dynamic viscosity, and kinematic viscosity, respectively; $\hat{p}$ denotes the generalized pressure including the hydrostatic pressure and the extra electrostrictive contribution [40]. The subscript l denotes liquid. The system is essentially governed by the following four dimensionless parameters:

$$T = \frac{\varepsilon(\phi_0 - \phi_1)}{\mu K}, \quad C = \frac{q_0 H^2}{\varepsilon(\phi_0 - \phi_1)}, \quad M = \frac{1}{K}\left(\frac{\varepsilon}{\rho}\right)^{1/2}, \quad \alpha = \frac{D}{K(\phi_0 - \phi_1)}. \tag{6}$$

The electric Rayleigh number T is defined as the ratio between the Coulomb force and the viscous force; C represents the injection strength; M is the nondimensional mobility parameter, which is the ratio of the so-called hydrodynamic mobility to the actual ionic mobility. From the definition equation, we know that M depends only on the physical properties of fluid. For dielectric liquids, its typical value is higher than 3 [40]; α is the nondimensional charge-diffusion number [41].

Macroscopic boundary conditions are given as: The horizontal electrodes (top and bottom) are considered to be rigid walls: $\mathbf{u} = 0$, $q = q_0$, $\phi = \phi_0$ at $y = 0$; $\mathbf{u} = 0$, $\partial q/\partial y = 0$, $\phi = \phi_1$ at $y = H$. The vertical boundaries (left and right) are assumed to be periodic for all fields.

B. Equations in the solid-liquid interface and solid region

The physical properties of solid substance have significant effects on not only the charge transport across the interface and electric field in the solid region, but also the liquid motion in the liquid region. In this study, two typical kinds of solid-liquid interfaces are considered distinguished by the charge-transport mechanism in the solid region, namely, the Ohmic solid and the non-Ohmic solid (see Fig. 1). In terms of the Ohmic solid, the current density in the solid phase obeys Ohm's law and the continuity of the electric current implies $K_l E_l q_l = \sigma E_s$ at the interface. Consequently, there will be surface charge accumulated at the solid-liquid interface $Q_s = \varepsilon_s E_s - \varepsilon_l E_l$. For the non-Ohmic solid, a mobility of the charges in the solid is considered (much smaller than that of the liquid $K_s \ll K_l$), and therefore the continuity of the electric current at the interface implies $K_l E_l q_l = K_s E_s q_s$. No surface charge will accumulate at the interface for the non-Ohmic solid and the continuity of the electric displacement vector gives $\varepsilon_s E_s = \varepsilon_l E_l$. For simplicity, we name the cases in the presence of the Ohmic solid and the non-Ohmic solid to be the "Ohmic case" and "non-Ohmic case," respectively. Due to the different charge-transport mechanisms in the solid region, equations for the Ohmic case and non-Ohmic one need to be separately provided as follows:

1. Ohmic model

At the solid region, equations are given as

$$\nabla \cdot (\varepsilon_s \nabla \phi) = -q_s, \quad \mathbf{E}_s = -\nabla \phi, \tag{7a}$$

$$\mathbf{J} = \sigma \mathbf{E}_s, \quad q_s = 0, \tag{7b}$$

$$\mathbf{u} = 0. \tag{7c}$$

At the solid-liquid interface, the continuity of the electric current must be satisfied, and the surface charge density can be calculated as

$$(K_l \mathbf{E}_l q_l - D_l \nabla q_l) \cdot \mathbf{n} = \sigma_s \mathbf{E}_s \cdot \mathbf{n}, \tag{8a}$$

$$(\varepsilon_s \mathbf{E}_s - \varepsilon_l \mathbf{E}_l) \cdot \mathbf{n} = Q_s, \quad (\mathbf{E}_s - \mathbf{E}_l) \times \mathbf{n} = 0. \tag{8b}$$

in which $\mathbf{n}$ is the unit vector normal to the surface and pointing towards the solid; σ_s is the electric conductivity at the solid phase. The subscripts s and i indicate the solid phase and interface, respectively.

2. Non-Ohmic model

At the solid domain, equations are given as

$$\nabla \cdot (\varepsilon_s \nabla \phi) = -q_s, \quad \mathbf{E}_s = -\nabla \phi, \tag{9a}$$

$$\frac{\partial q_s}{\partial t} + \nabla \cdot (K_s \mathbf{E}_s q_s - D_s \nabla q_s) = 0, \tag{9b}$$

$$\mathbf{u} = 0. \tag{9c}$$

At the solid-liquid interface, the continuity of both the electric current and electric displacement vector must be satisfied:

$$(K_l \mathbf{E}_l q_l - D_l \nabla q_l) \cdot \mathbf{n} = (K_s \mathbf{E}_s q_s - D_s \nabla q_s) \cdot \mathbf{n}, \tag{10a}$$

$$(\varepsilon_s \mathbf{E}_s - \varepsilon_l \mathbf{E}_l) \cdot \mathbf{n} = 0 \quad (\mathbf{E}_s - \mathbf{E}_l) \times \mathbf{n} = 0. \tag{10b}$$

Three more parameters need to be considered due to the presence of the solid-liquid interface. In the Ohmic case, a nondimensional electric conductivity S is defined to be the ratio between conductivity in the solid and the mobility in the liquid. In the non-Ohmic model, two parameters ε_r and K_r are considered, defined to be the ratios of permittivity and mobility between the liquid and solid phases. In addition, a geometric parameter named interface position f_l is defined as the liquid layer thickness H_l versus electrode distance H, expressed as

$$S = \frac{\sigma}{K_l q_0}, \quad \varepsilon_r = \frac{\varepsilon_l}{\varepsilon_s}, \quad K_r = \frac{K_l}{K_s}, \tag{11a}$$

$$f_l = \frac{H_l}{H}. \tag{11b}$$

C. The lattice Boltzmann model

Instead of directly solving the complex macroscopic equations, an improved LBM is developed to simulate this problem based on three well-designed LBEs for electric potential, charge density, and flow field [32,42], respectively. The numerical scheme is inherited from our previously developed unified lattice Boltzmann model (ULBM) for single-phase electroconvective flow. For different physical fields, our ULBM uses the same forms of LBEs, equilibrium distribution function, and relaxation time. A unique advantage of our ULBM lies in simple, efficient, and easy modular programming.

When considering the interface, the LBEs for charge density and flow field can be naturally adapted by using the modified equilibrium distribution and bounce-back scheme, respectively. However, the LBE for electric potential in ULBM fails in dealing with the Ohmic case due to the discontinuity of the electric displacement vector $\varepsilon \mathbf{E}$ at the interface; in consequence, the code for electric potential has been rewritten. Detailed equations are given as follows.

1. LBM for electric potential

To solve the electric potential in the presence of solid-liquid interface for both the non-Ohmic and Ohmic cases, an improved lattice Boltzmann model for the Poisson equation proposed by Chai and Shi [43] is added to our LBM system. In this model, the artificial transient term derived by previous models is eliminated. The corresponding LBE can be given as

$$g_j(\mathbf{x}+\mathbf{c}_j\Delta t, t+\Delta t) - g_j(\mathbf{x},t) = -\frac{1}{\tau_\phi}\left[g_j(\mathbf{x},t) - g_j^{eq}(\mathbf{x},t)\right] + \Delta t\varpi_j R D_a, \tag{12}$$

where g, $\mathbf{c}$, τ_ϕ, R, D_a are the distribution function, the microscopic velocity, relaxation time, source term, and artificial diffusion coefficient, respectively. The D2Q5 velocity discretization scheme is adopted with the equilibrium distribution function g_j^{eq} and D_a corresponding weight coefficients ω and ϖ are expressed as

$$g_j^{eq}(\mathbf{x},t) = \begin{cases} (\omega_0 - 1.0) & j=0 \\ \omega_j\phi & j=1-4 \end{cases}, \quad \omega_j = \begin{cases} 0 & j=0 \\ 1/4 & j=1-4 \end{cases}, \quad \varpi_j = \begin{cases} 0 & j=0 \\ 1/4 & j=1-4 \end{cases}. \tag{13}$$

In this work, we use a local permittivity-dependent relaxation time τ_ϕ is computed by

$$\tau_\phi = \frac{\varepsilon_t D_a}{\beta c^2 \Delta t} + \frac{1}{2}, \tag{14}$$

where ε_t $(=\varepsilon/\varepsilon_l)$ is the ratio between the local permittivity ε and the liquid permittivity ε_l, the artificial diffusion coefficient $D_a(D_a > 0)$ is chosen to be $D_a = 1/2$ in our simulations in balance of evolution speed and stability. The coefficient β has been derived to be $1/2$ by the Chapman-Enskog expansion [43]. Then, the source term R can be given as

$$R = q/\varepsilon. \tag{15}$$

Finally, the electric potential can be evaluated as

$$\phi = \frac{1}{1-\omega_0}\sum_{j=1}^{4} g_j. \tag{16}$$

To calculate the electric field $\mathbf{E}$ in Eqs. (2), (7a), and (9a), a straightforward way is to use the second-order central differencing formula for a gradient. But in this study, we obtain the electric field $\mathbf{E}$ by a totally local manner with the help of distribution function g, which avoids the complex treatment in obtaining the electric field at the solid-liquid interface,

$$\mathbf{E} = \frac{1}{\tau_\phi \beta \Delta t}\sum_j \mathbf{c}_j g_j. \tag{17}$$

In LBM simulations, our code can naturally distinguish the electric potential and electric field between the liquid and solid regions, which is due to the local permittivity-related relaxation time in Eq. (14) and the local way to compute the electric field as in Eq. (17).

2. LBM for flow field

The LBE for the flow motion in the liquid phase can be expressed as [44]

$$f_j(\mathbf{x}+\mathbf{c}_j\Delta t, t+\Delta t) - f_j(\mathbf{x},t) = -\frac{1}{\tau_v}\left[f_j(\mathbf{x},t) - f_j^{eq}(\mathbf{x},t)\right] + \Delta t \times F_j, \tag{18}$$

where f, τ_v, F_j are the distribution function, the relaxation time, and Coulomb force term, respectively. The D2Q9 velocity discretization scheme [30] is adopted with the equilibrium distribution

function f_j^{eq} and corresponding weight coefficients ω are expressed as

$$f_j^{eq} = \rho\omega_j\left(1 + \frac{\mathbf{c}_j \cdot \mathbf{u}}{c_s^2} + \frac{(\mathbf{c}_j \cdot \mathbf{u})^2}{2c_s^4} - \frac{u^2}{2c_s^2}\right), \quad \omega_j = \begin{cases} 4/9 & j = 0 \\ 1/9 & j = 1-4 \\ 1/36 & j = 5-8 \end{cases}. \tag{19}$$

The relaxation time τ_v is computed from [30]

$$\tau_v = \frac{3\nu}{c^2\Delta t} + \frac{1}{2}. \tag{20}$$

The Coulomb force term in Eq. (18) can be calculated in every discretization direction from

$$F_j = \omega_j\left(1 - \frac{1}{2\tau_v}\right)\frac{\mathbf{c}_j q\mathbf{E}}{c_s^2}. \tag{21}$$

Finally, the fluid mass density ρ the velocity $\mathbf{u}$ can be evaluated from Eq. (22):

$$\rho = \sum_j f_j \quad \rho\mathbf{u} = \sum_j \mathbf{c}_j f_j + \frac{\Delta t}{2} q\mathbf{E}. \tag{22}$$

Due the no-slip condition at the solid-liquid interface, the classical bounce-back scheme is adopted at both the interface and solid region.

3. LBM for charge density

The LBE for charge density has been derived in our previous single-phase electroconvection, given as

$$h_j(\mathbf{x} + \mathbf{c}_j\Delta t, t + \Delta t) - h_j(\mathbf{x}, t) = -\frac{1}{\tau_q}\left[h_j(\mathbf{x}, t) - h_j^{eq}(\mathbf{x}, t)\right], \tag{23}$$

with the equilibrium distribution function h_j^{eq} given as

$$h_j^{eq}(\mathbf{x}, t) = q\omega_j\left\{1 + \frac{\mathbf{c}_j(K\mathbf{E} + \mathbf{u})}{c_s^2} + \frac{[\mathbf{c}_j(K\mathbf{E} + \mathbf{u})]^2 - c_s^2(K\mathbf{E} + \mathbf{u})^2}{2c_s^4}\right\}. \tag{24}$$

The D2Q9 model is used with ω_j defined in Eq. (19). The relaxation time in Eq. (23) is defined as

$$\tau_q = \frac{3D}{c^2\Delta t} + \frac{1}{2}, \tag{25}$$

where D is the charge-diffusion coefficient expressed in Eq. (3). The charge density is evaluated from

$$q = \sum_j h_j. \tag{26}$$

The LBM code identifies the liquid and solid regions by the mobility and charge-diffusion coefficient differences in these two regions, which are involved in the equilibrium distribution [Eq. (23)] and the relaxation time [Eq. (24)], respectively.

The mesoscopic boundary conditions and interface treatment scheme are presented in Appendix A. For the purpose of code validation, the analytical solutions at hydrostatic state for both the Ohmic and non-Ohmic cases are also derived in Appendix B. Numerical results are presented by isosurfaces and streamlines, as well as the electric Nusselt numbers (Ne), given as

$$Ne = I/I_0, \tag{27a}$$

$$I = \frac{1}{L}\int_0^L \left[q(E_y + u_y) + \frac{\partial E_y}{\partial t}\right]\Big|_{y=0 \text{ or } y=1} dx, \tag{27b}$$

$$I_0 = (qE_y|_{y=0 \text{ or } y=1})_{\text{hydrostatic state}}. \tag{27c}$$

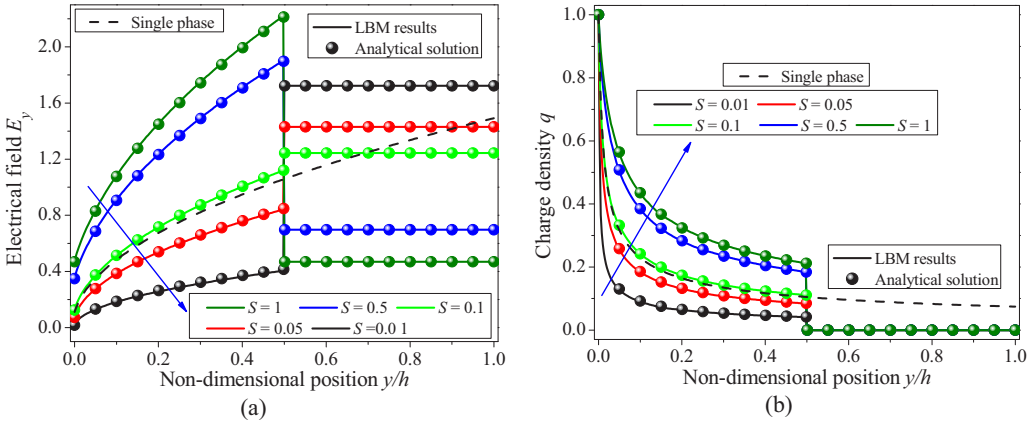

FIG. 2. Validation of LBM model for the Ohmic cases at hydrostatic state: (a) electric field at y direction E_y and (b) charge-density distributions for different electric conductivity S. Dashed line is the results of single-phase problem.

III. RESULTS AND DISCUSSION

In this section, the LBM code is first validated by comparing with the analytical results at hydrostatic state. Then, a comprehensive numerical study of electroconvection in the presence of solid-liquid interface is conducted. Simulations are performed for both the Ohmic and non-Ohmic models. The effects of the interface position f_l, nondimensional electric conductivity S, permittivity, and mobility ratios ($\varepsilon_r K_r$) on the flow patterns and bifurcations are investigated. In all simulations, a strong charge injection $C = 10$ is considered, and the mobility and charge diffusion are fixed at $M = 10$ and $\alpha = 10^{-4}$, respectively. The aspect ratio of the computational domain is set to be $A = L/H = 1.228$ and a grid discretization scheme with 246×200 lattices in a cavity computational domain is adopted.

A. Code validation

Without the flow motion (by setting velocity to be zero or under small values of the driving parameter $T < T_c$), the problem can be reduced to the electric field–space charge coupled problem governed by Eqs. (1)–(3), also known as the hydrostatic solution. The hydrostatic solution of single-phase model has been derived for zero and nonzero value of charge-diffusion coefficient [9,45,46]. The hydrostatic solutions in the presence of the solid-liquid interface are derived in this work as given in Appendix B.

1. The Ohmic case

The hydrostatic solution of the Ohmic case depends on the nondimensional electric conductivity S and interface position f_l. Figure 2 presents the electric-field component E_y and charge-density q distributions under different S. As shown in Fig. 2(a), a discontinuity in the distribution of E_y can be readily observed at the interface due to the nonzero surface charge accumulation Q_s. Besides, the value of E_y in liquid phase increases as the increase of S, but an opposite trend is observed in the solid phase. As presented in Fig. 2(b), charge density q also increases with S increasing in the liquid phase, but q suddenly decreases to zero at the interface as no free charge exists in the solid phase for the Ohmic case.

The influence of interface position f_l on electric field E_y and charge density q is shown in Figs. 3(a) and 3(b), respectively. It is seen that both E_y and q slightly increase as increasing of f_l in the liquid phase. Besides, for all test cases presented in Figs. 2 and 3, our LBM results show

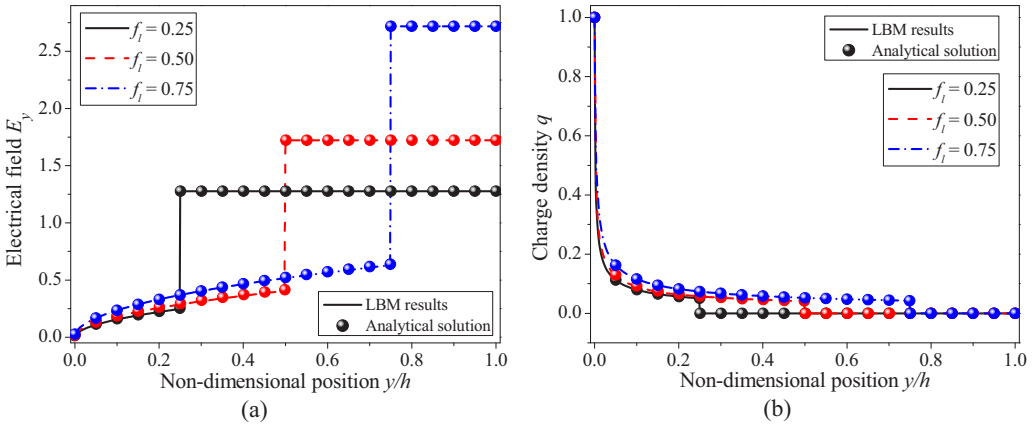

FIG. 3. (a) Electric-field E_y and (b) charge-density q distributions for different interface position f_l for the Ohmic cases at $S = 0.01$.

an excellent agreement with the analytical solutions. In particular, the LBM code well reproduces the discontinuity of the electrical field E_y and charge density q.

2. The non-Ohmic case

No free charge will accumulate at the interface in this case, and the continuities of both the electric current and electric displacement vector at interface imply $K_l E_l q_l = K_s E_s q_s$ and $\varepsilon_s E_s = \varepsilon_l E_l$, respectively. However, the difference of permittivity and mobility $(\varepsilon_r K_r)$ between the liquid and solid regions will result in the discontinuities in the distributions of E_y and q. Therefore, three representative cases with different combinations of $(\varepsilon_r K_r)$ are tested. As shown in Fig. 4, for $\varepsilon_r = 1$ and $K_r = 1$, the results are the same as the single-phase problem. Both the electric field E_y and charge density q show continuous distributions in the whole domain. For the case $\varepsilon_r = 2$ and $K_r = 1$, a sudden jump can be observed at the interface in electric field E_y; see Fig. 4(a). In detail, the values of E_y in the liquid side is half of that in the solid side, opposite to the value of permittivity ratio ε_r, which satisfies the relationship given in Eq. 10(b).

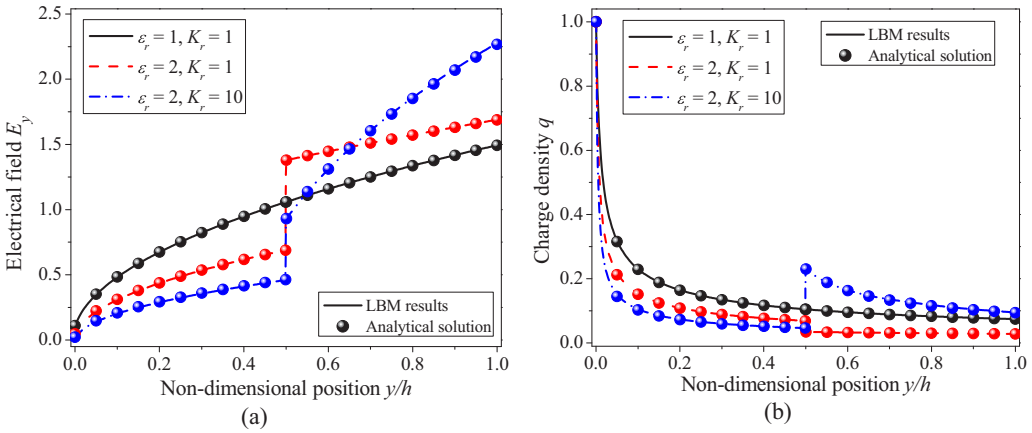

FIG. 4. Validation of LBM model for the non-Ohmic cases at hydrostatic state: (a) electric-field E_y and (b) charge-density distributions for different combinations of permittivity ratio and mobility ratio $(\varepsilon_r K_r)$.

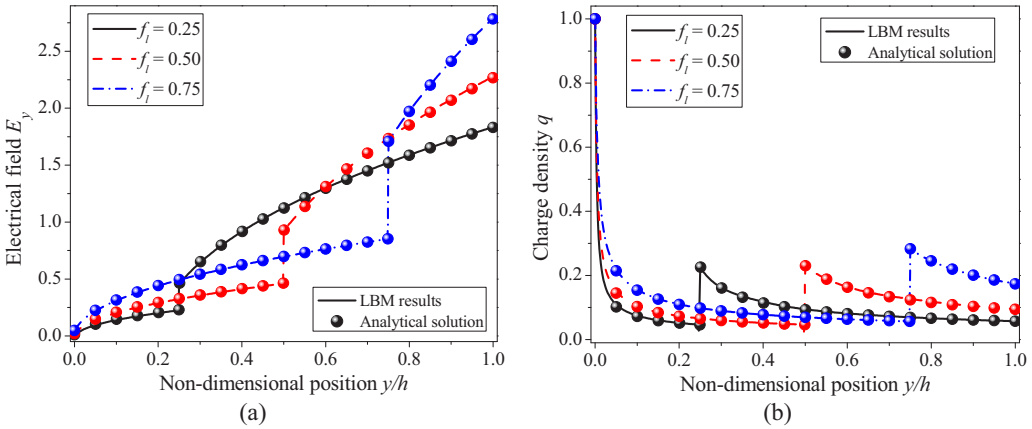

FIG. 5. (a) Electric-field E_y and (b) charge-density q distributions for different interface position f_l for the non-Ohmic cases at $\varepsilon_r = 2$ and $K_r = 10$.

Meanwhile, as shown in Fig. 4(b), a sudden decrease at the interface can be observed in q profiles, which is due to the conservation of charge density as given in Eq. 10(a). However, for the case $\varepsilon_r = 2$ and $K_r = 10$, a sudden jump of q at the interface can be obtained in Fig. 4(b), which can be explained by the fact that a relatively lower mobility K in the solid phase requires a higher charge density q to satisfy the continuity condition of electric current density. Besides, with the increase of ε_r or K_r, both charge density and electric field have lower values in the liquid phase. Figure 5 shows the effects of interface position f_l on E_y and q distributions. It is seen that both E_y and q have larger values in liquid phase for a larger f_l. For all non-Ohmic cases presented in Figs. 4 and 5, the numerical results fit well with the analytical solutions with the maximum difference less than 1%.

B. Electroconvection with solid-liquid interface

When electric Rayleigh number T exceeds its linear stability threshold $T > T_c$, the Coulomb force is strong enough to overcome the damping action of the viscous force and the convective flow will be motivated from the motionless state. As shown in Fig. 6, some basic features of electroconvection, such as the charge void region in charge-density distributions and vortices pairs, can be clearly observed for both Ohmic and non-Ohmic cases in Figs. 6(a) and 6(b), respectively. Compared to the single-phase electroconvection, the presence of solid-liquid interface leads to much more complex distribution of charge density and different number of flow vortices.

To better illustrate the charge void region and discontinuous distribution in charge density field, simulation results of q are presented in the forms of 3D contours with z-axis being charge density (left side). The charge void region is formed due to the competition between the migration and convection mechanisms for charge transport [8], and the discontinuities of q is due to the interface effect. For both Ohmic and non-Ohmic cases [Figs. 6(a) and 6(b)], two complete charge void regions in the liquid phase can be observed, which can be explained by the fact that the aspect ratio of liquid region $A = L/(Hf_l) \approx 2.46$ is close to twice the critical wavelength of the most unstable mode ($\lambda_c = 1.228$). However, significant difference can be observed in the q distribution in the solid phase. There is a sudden decrease to zero at the interface of the Ohmic case while there is a jump increase in the non-Ohmic situation, which is consistent with the hydrostatic solutions shown in Figs. 2(b) and 4(b), respectively. Besides, streamlines of convection together with electric field are also plotted in Fig. 6. It is seen that the flow motion exhibits a two-pairs of vortices pattern in the liquid region for both the Ohmic and non-Ohmic cases, but the nondimensional stream function *Str* has a larger value in the Ohmic case implying the relatively stronger flow strength.

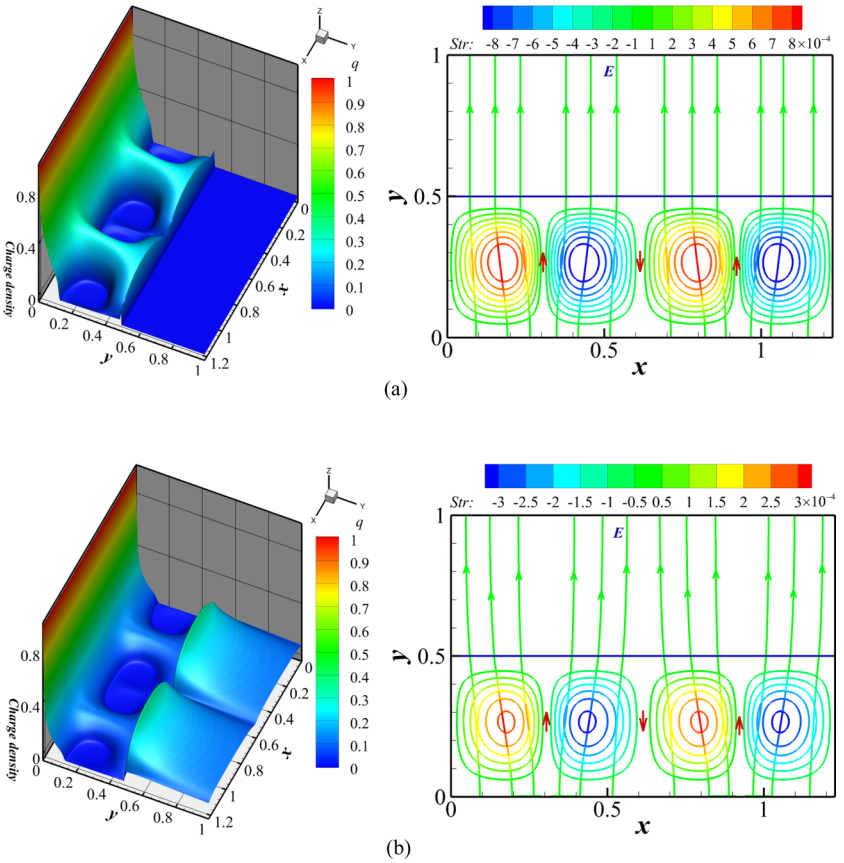

FIG. 6. Results of electroconvection for (a) the Ohmic cases at $T = 500$, $S = 0.1$, and (b) the non-Ohmic cases at $T = 1200$, $\varepsilon_r = 2$, $K_r = 10$. In each figure, the left contour map is the charge-density distribution while the right plot is the dimensionless stream function *Str* with electric field $\boldsymbol{E}$.

Another representative characteristic of electroconvection of single-phase liquid lies in its subcritical bifurcation in the finite-amplitude regime. Here we are interested in the bifurcation behavior in the presence of the solid-liquid interface. The bifurcation diagrams of Ohmic and non-Ohmic cases expressed by the electric Nusselt number *Ne* versus T are presented in Figs. 7(a) and 7(b), respectively. It is seen that both bifurcations are of subcritical type, featured by a linear stability criterion T_c, a finite-amplitude stability criterion T_f (also called a nonlinear stability criterion), and a hysteresis loop linking the two criteria. In our numerical practice, T_c is decided by the interpolation of growth rate at the exponential stage, which has been well addressed in our previous work [47]. T_f is determined as follows. Restart the computation from a steady convection obtained with T slightly higher than T_c, then gradually decrease T by a small amount until a critical value (i.e., T_f), at which the system suddenly jumps from a convective state of finite-amplitude strength to the rest state. For Ohmic and non-Ohmic cases, our numerical findings of T_c are 456.7 and 1072.1, and T_f are 311.9 and 783.6, respectively.

It is seen that both T_c and T_f are larger than the corresponding values with single-phase electroconvection (164.1 and 111.7 [8]). This can be explained by the fact that a voltage drop happens at the solid region leading to a higher requirement of applied voltage between the electrodes to motivate the electroconvection. In detail, the useful voltage drop in the liquid layer is but a fraction of the total voltage drop. Let us define this voltage drop as V_l in the hydrostatic state, which may be

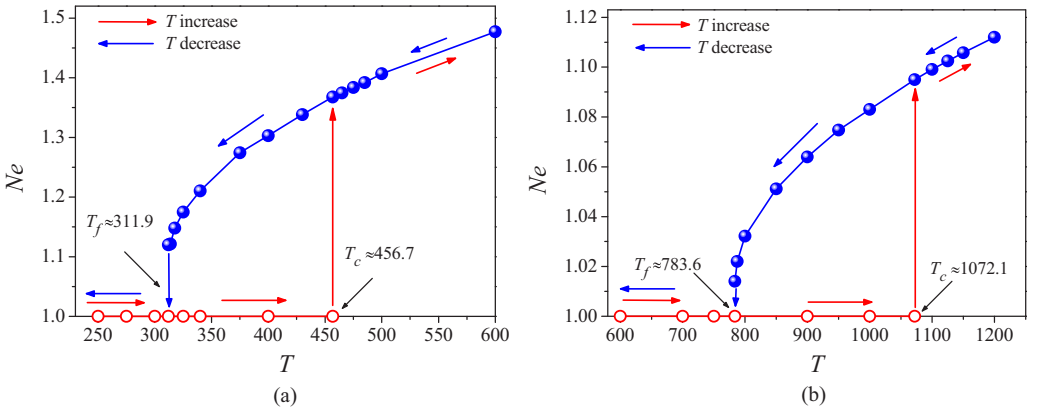

FIG. 7. The subcritical bifurcation diagram of electroconvection with solid-liquid interface: (a) Ohmic case at $S = 0.1$ and (b) non-Ohmic case at $\varepsilon_r = 2$ and $K_r = 10$.

computed from the analytical solution. For the Ohmic case, the voltage drop V_l is 0.3782 at $S = 0.1$, $f_l = 0.5$, while for the non-Ohmic one $V_l = 0.1547$ at $K_r = 10$, $\varepsilon_r = 2$, and $f_l = 0.5$. By combining with the definition of electric Rayleigh number T, we have that the relation between the T parameter across the layer T_l and across the whole system is $T = T_l/V_l$. Taking $T_{lc} = 164.1$ as the expected critical value for the liquid layer alone [8], we obtain 434 and 1061 as the ideal values for T, to be compared with the numerically obtained 456.7 and 1072.1. The differences are attributable to that the upper boundary is no longer an equipotential surface and also that the aspect ratio of the convective cells does not correspond to the most unstable mode for f_l does not equal to 1.

C. The effects of solid-liquid interface position f_l

In this part, we further consider the effects of interface position f_l on flow pattern and related bifurcations. Figure 8 shows the stability map of both the Ohmic and non-Ohmic cases based on a large number of the computational runs with wide ranges of the electric Rayleigh number $T(100 \sim 25\,000)$ and the interface positions f_l $(0.1 \sim 0.9)$. In each figure, a dash-dot line separates the whole domain into a stable region and an unstable one. In the stable region, the Coulomb force

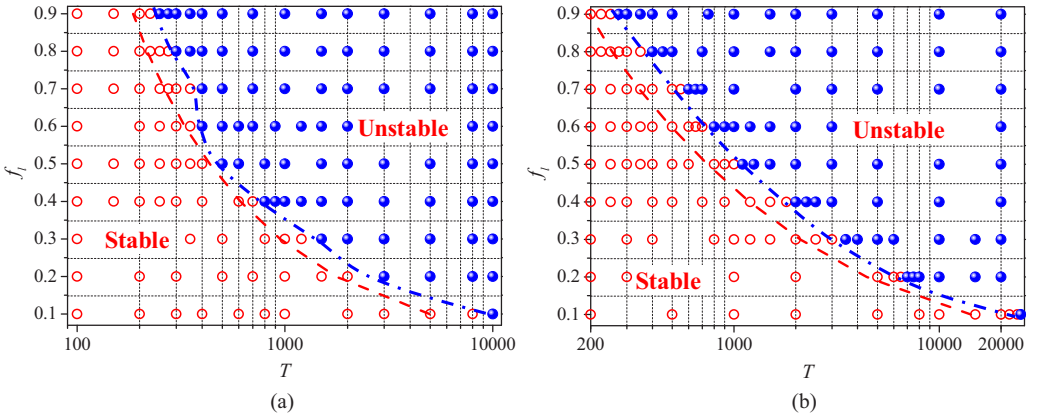

FIG. 8. Regions of stable and unstable in electroconvection under different interface position f_l for the (a) Ohmic model at $S = 0.1$ and (b) non-Ohmic model at $\varepsilon_r = 2$ and $K_r = 10$.

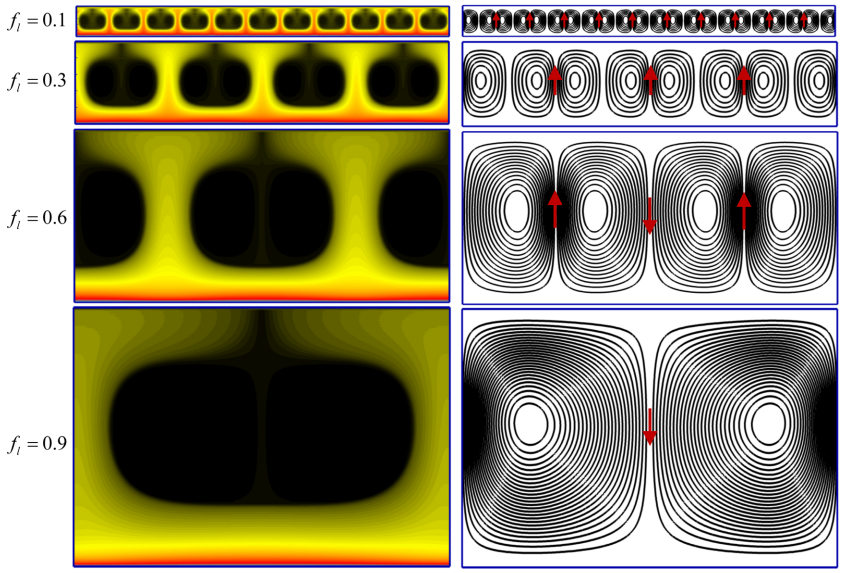

FIG. 9. The steady-state charge-density distributions and streamlines at four interface position $f_l = 0.1$, 0.3, 0.6, and 0.9 for the Ohmic cases. Results are presented only in the liquid region as $q = 0$ and $\mathbf{u} = 0$ at the solid phase.

is unable to overcome the damping action of the viscous force, and the fluid remains in a motionless state, marked by the hollow circle in Fig. 8. This static state is potentially unstable; once T is across the dashed line (linear stability curve), the system loses its linear stability and the flow motion arises, evolving into convective flow patterns as shown in Figs. 9 and 10.

Another dashed line in Fig. 8 indicates the theoretically predicted values of T_c, computed by the ratio of critical value T_{lc} in single-phase electroconvection and voltage drop V_l at hydrostatic state. Obviously, the numerically predicted T_c values (dash-dot line) are systematically above the theoretical ones (dashed line) as presented in Fig. 8, which may be explained by the fact that the aspect ratio for the theoretical case corresponding to the most unstable at $f_l = 1$ is not general for other values of f_l. For instance, as shown in Fig. 9, for $f_l = 0.9$ the aspect ratio of just a pair of convective cells is $L/H_l = L/(f_l H) = 1.364$; for $f_l = 0.6$ we have two pairs of convective cells of 1.023 aspect ratio; for $f_l = 0.3$ we have three pairs of cells and the aspect ratio is again 1.364; and for $f_l = 0.1$ we observe ten pairs of cell with an aspect ratio of 1.228. Moreover, the interface in a real situation is no longer an equipotential surface as assumed in the theoretical case. Therefore, the values of T_c are higher than the theoretical ones. As shown in Fig. 8, the stability map for both the Ohmic and non-Ohmic cases have similar trends, such as the linear stability criteria T_c increase as the decreasing of f_l in both cases due to the reason that a thicker solid layer will induce a larger useless voltage drop in the solid region. However, there are some differences between Figs. 8(a) and 8(b). For instance, the stability curve of the non-Ohmic case has smoother distribution than that of Ohmic ones. In addition, the values of T_c for the non-Ohmic case, varying from $T_c \approx 250$ at $f_l = 0.9$ to $T_c \approx 24\,000$ at $f_l = 0.1$, are larger than those of the Ohmic case, $T_c \approx 237$ at $f_l = 0.9$ to $T_c \approx 9000$ at $f_l = 0.1$.

The final steady-state charge-density distribution and velocity field of the Ohmic case at four representative cases are presented in Fig. 9; from top to bottom, parameters are set to be ($f_l = 0.1$, $T = 12000$), ($f_l = 0.3$, $T = 1400$), ($f_l = 0.6$, $T = 450$), and ($f_l = 0.9$, $T = 300$), respectively. In those cases, the governing parameters T are chosen to be slightly above the corresponding linear stability criterion T_c to avoid the secondary instability. Results are presented only in the liquid region as both the charge density and velocity are zero at the solid phase. As shown in Fig. 9, the charge

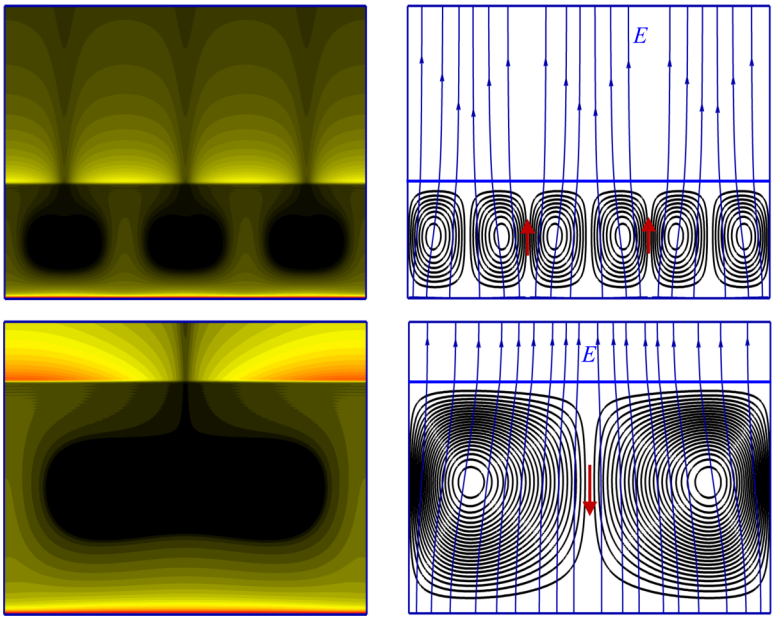

FIG. 10. The steady-state charge-density distributions and streamlines at two different interface position $f_l = 0.4$, and 0.8 for the non-Ohmic cases.

density and streamlines have similar shapes for different f_l but the number and the size of the charge void region and vortices are different. For a smaller f_l, the aspect ratio of liquid region $A = L/(Hf_l)$ is larger, and therefore the flow pattern with more periodic units can be motivated. Quantitatively, 11, 4, 2, and 1 basic periodic units (1 periodic unit including 1 charge void region and 2 vortices) can be observed for the cases $f_l = 0.1$, 0.3, 0.6, and 0.9, respectively. Besides, distributions of charge density and velocity for two cases with parameters ($f_l = 0.4$, $T = 2000$) and ($f_l = 0.8$, $T = 500$) are considered for the non-Ohmic cases. As shown in Fig. 10, a sudden increase in charge-density distribution happens at the interface; three and one periodic units can be observed in the liquid phase at $f_l = 0.4$ and $f_l = 0.8$, respectively.

D. The effects of electric conductivity S, permittivity ratios ε_r, and the mobility ratios K_r

As presented in Eqs. (6) and 11(a), there are seven nondimensional parameters (T, C, M, α, S, ε_r, K_r) in this problem except for the geometry parameters. Among them, the first four (T, C, M, α) are common parameters in both the single-phase and two-phase electroconvection problems. The effects of (T, C, M, α) on flow instability and bifurcations have been well discussed in previous works on single-phase problems [9,45,48,49]. Here we consider the additional three parameters

TABLE I. Numerical predictions of the linear and finite-amplitude stability criteria T_c and T_f under different S.

Electric conductivity S in solid phase	0.01	0.05	0.1	0.5	1
Linear stability criteria T_c	1190.0	594.4	456.7	296.0	265.9
Finite-amplitude stability criteria T_f	857.1	409.6	311.9	192.9	170.0

TABLE II. Linear and finite-amplitude stability criteria T_c and T_f for various values of ε_r at $K_r = 1$.

Ratios of permittivity between solid and liquid phase ε_r	1	2	3	4	5
Linear stability criteria T_c	487.9	731.4	954.1	1191.2	1398.1
Finite-amplitude stability criteria T_f	331.7	502.5	671.9	850.8	1019.5

(S, ε_r, K_r) in the presence of a solid-liquid interface; results are provided for the effect of (S, ε_r, K_r) on the linear and finite-amplitude stability criteria of convective flow.

For the Ohmic case, only S needs to be considered as defined in Eq. (11a). As shown in Table I, both T_c and T_f decrease as the increasing of S. Due to the reason that a larger S corresponds to a lower electrical resistance $R = 1/S$, which induces a smaller voltage drop in the solid phase, consequently convective flow takes place at a relative lower T_c. Particularly, the two limiting cases, $S \to 0$ and $S \to \infty$, represent the totally insulating solid and perfect conductor, respectively. In the first case, there is no electric current in the system and therefore electroconvection will never be motivated; therefore $T_c \to \infty$. And in the latter case, the solid layer can be considered to be a part of the electrode and the problem will degenerate into the single-phase electroconvection problem with stability criteria $T_c \approx 164.1$ and $T_f \approx 111.7$. In addition, the variation of T_f with S has a similar trend as T_c, but the gap between T_f and T_c, expressed by $g = T_c/T_f$ becomes larger with the increase of S, as presented in Table I, which means a larger nondimensional voltage drop is required to recover the system from the convective state to the motionless state at a larger S.

For the non-Ohmic case, both the permittivity ratios ε_r and the mobility ratios K_r between the liquid and solid phase have significant effect on electroconvective instability. Results about the effects of ε_r and K_r are presented in Tables II and III, respectively. As shown in Table II, both the stability criteria T_c and T_f increase as the increasing of ε_r, which can be simply interpreted that as the continuity of that electric displacement vector at the interface gives $E_s/E_l = \varepsilon_r$, and a larger ε_r corresponds to a relatively larger electric field E_s and a larger voltage drop in the solid phase, therefore a larger applied voltage is required to motivate the electroconvection in the liquid layer. Besides, the basic mechanism of the influence of $K_r(=K_l/K_s)$ on stability criteria is the same as the electrical resistance $R[=1/S = K_l/(\sigma/q_0)]$ in the Ohmic case, and the only difference is the type of charge carrier in the solid phase. Therefore, both T_c and T_f increase as K_r increases as shown in Table III.

IV. CONCLUSIONS

In this paper, electroconvection of dielectric liquids subjected to a solid-liquid interface has been numerically studied. A physical model with fully coupled mathematical equations has been built for both the Ohmic and non-Ohmic models with the solid phase. An improved lattice Boltzmann model (LBM) has been developed. An interface treatment for conjugate charge transport is proposed based on the half-lattice division scheme. The continuity of electric current and electric displacement vector is intrinsically satisfied without iterative computations, and the interfacial electric field is conveniently obtained by a local manner from the microscopic distribution functions.

TABLE III. Linear and finite-amplitude stability criteria T_c and T_f for various values of K_r at $\varepsilon_r = 1$.

Ratios of mobility between solid and liquid phase K_r	1	2	5	10	50
Linear stability criteria T_c	487.9	530.5	635.4	767.4	1364.4
Finite-amplitude stability criteria T_f	331.7	366.2	447.5	551.2	1333.4

The numerical model and the interface treatment scheme have been fully validated by the hydrostatic solutions. Good agreement between numerical and analytical solutions is always obtained for both the Ohmic and non-Ohmic model. Then, simulations have been conducted for electroconvective flows under different governing parameters, and results are presented for flow pattern, bifurcation diagram, and stability map. Numerical results have revealed that (1) the bifurcation of electroconvection with a solid-liquid interface are of subcritical type; for both the Ohmic and non-Ohmic cases, the linear and nonlinear stability thresholds (T_c and T_f) are larger than those of single-phase electroconvection problem as a useless voltage drop happening at the solid phase; and (2) the value of T_c increases as the permittivity ratios ε_r and mobility ratios K_r increases, but T_c decreases with the increaseing of nondimensional electric conductivity S and interface position f_l.

The present study extends the previous work of electroconvection from single-phase dielectric liquid to the solid-liquid interaction problem. The numerically obtained linear and nonlinear stability criteria can serve as reference for future theoretic stability analysis. In addition, our work may provide some theoretic basis for electrohydrodynamic phase-change heat transfer in the next work.

ACKNOWLEDGMENTS

This work is supported by the National Natural Science Foundation of China (Grants No. 51776054, No. 51906051, and No. 11802079), and partially by financial support by Spanish Goverment Agency Ministerio de Economia y Competitividad [Contract No. CTQ2017-83602-C2 (MINECO-FEDE)] and National Postdoctoral Program for Innovative Talents of China (Grant No. AUGA4150000117).

APPENDIX A: MESOSCOPIC BOUNDARY CONDITIONS AND INTERFACE TREATMENT

The macroscopic boundary conditions have been provided in Sec. II A. For the lattice Boltzmann simulation, the treatment of mesoscopic boundary conditions is also a key issue. For the left and right boundaries, the periodic boundary condition can be easily achieved in LBM by setting distribution functions that leave the computational domain from one side and reenter from the opposite side [47]. At the up and bottom electrodes, the bounce-back scheme [50] is used for the flow field, while the nonequilibrium extrapolation scheme [51] is adopted for other fields.

$$g_j(\mathbf{r_b}, t) = g_j^{eq}(\mathbf{r_b}, t) + \left[g_j(\mathbf{r_f}, t) - g_j^{eq}(\mathbf{r_f}, t)\right]. \tag{A1}$$

The treatment of the solid-liquid interface is also a key issue. As shown in Fig. 11, a half-lattice division scheme in which the interface is placed on the middle point between the fluid and solid nodes is adopted [37]. The advantage of this scheme is that no lattice node is located at the interface. It can be seen from Fig. 11 that the lattice links marked in red will cross the interface with nodes in the liquid side, and solid side are marked to be $\mathbf{x}_l$ and $\mathbf{x}_s$, respectively.

In LBM simulations, the interface equations [expressed through Eqs. (8) and (10)] should be satisfied. For the non-Ohmic case, simulations are conducted for the whole domain including the solid and liquid region; our lattice Boltzmann code can naturally satisfy the relationship [Eq. (10)] by special techniques in different LBEs in detail as shown in Fig. 11(a): the bounce-back scheme in the solid region for the flow field, the local permittivity-related relaxation time for electric potential [Eq. (14)], and the mobility-related equilibrium distribution for charge density [Eq. (24)].

For the Ohmic solid, there is no charge density in the solid region as discussed in a mixed model [52], i.e., $q_s = 0$. Consequently, electric field in the solid region has a constant value $E_s = c$ by solving Eq. (7a). Then, the electric potential in the solid region has a linear distribution, $\phi_s = \phi_1 + c(H - y)$. Therefore, simulations are merely conducted in the liquid region, with the interface equations [Eq. (8)] being regarded as the boundary condition. By defining the nondimensional electric conductivity to be $S = \sigma_s/(K_l q_0)$, the boundary condition for electric potential can be given

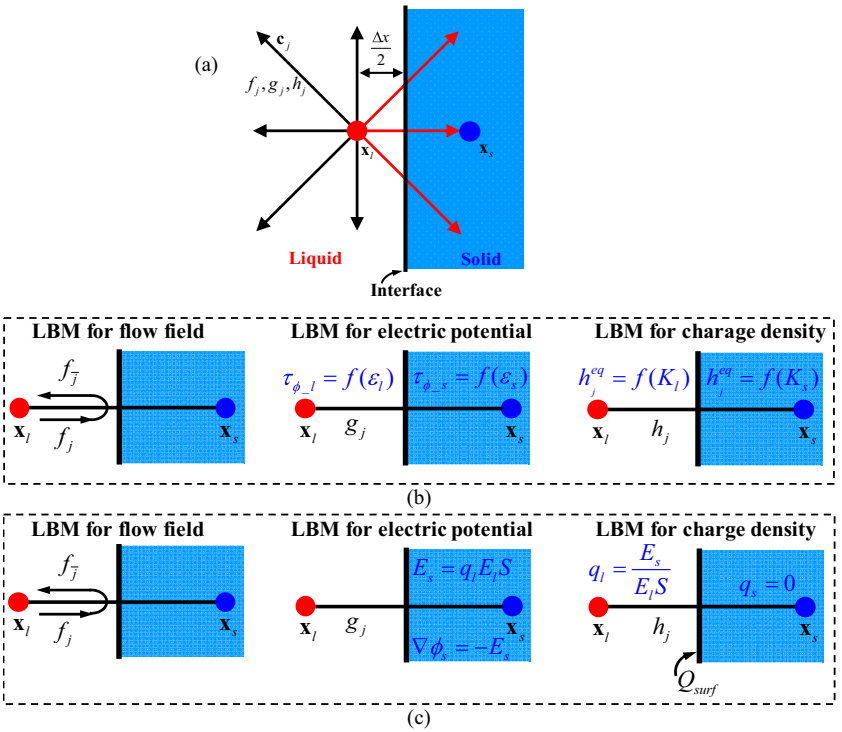

FIG. 11. The solid-liquid interface treatment scheme. (a) The sketch of half-lattice division scheme. (b) The sketch of interface treatments for different fields for the non-Ohmic case. (c) the sketch of interface treatments for the Ohmic solid case.

as

$$\phi_s = \phi_1 + \frac{q_l E_l (H - y)}{S q_0}, \tag{A2}$$

where q_l and E_l are the values of charge density and electric field at the liquid side of the interface [$\mathbf{x}_l$ in Fig. 11(a)], respectively, which can be obtained from the previous iteration step. Besides, the zero-slope condition is assumed for charge potential at the interface, expressed as

$$\partial q / \partial y = 0. \tag{A3}$$

APPENDIX B: DERIVATION OF ANALYTICAL SOLUTIONS

The hydrostatic solution of THE single-phase model has been derived for zero and nonzero values of charge-diffusion coefficient [9,45,46]. However, in the presence of solid-liquid interface, no analytical solution can be found. In this section, analytical solutions for both the non-Ohmic and Ohmic solid models are provided.

1. Analytical solution for the Ohmic model

In the liquid phase, analytical solutions of electric-field and charge-density distributions are expressed as

$$E_l = a(y + b)^{1/2}, \quad q_l = \frac{a}{2C(y + b)^{1/2}}. \tag{B1}$$

In the solid phase, analytical solution are given as

$$E_s = c \quad q_s = 0. \tag{B2}$$

The constants a, b, c, d can be obtained by solving the following coupled algebraic equations:

$$a = 2Cb^{1/2},$$

$$c = 2Cb/S, \quad S = \sigma/(K_l q_0),$$

$$\frac{2}{3}2Cb^{1/2}[(f_l + b)^{3/2} - b^{3/2}] + \frac{2Cb}{S}(1 - f_l) - 1 = 0,$$

$$Q_s = \frac{2Cb\varepsilon_r}{S} - 2Cb^{\frac{1}{2}}(f_l + b)^{1/2},$$

where $\varepsilon_r = \varepsilon_l/\varepsilon_s$ and $K_r = K_l/K_s$ are the ratios of permittivity and mobility between the liquid and solid phases, respectively. The liquid fraction f_l indicates the position of the solid-liquid interface (defined to be the ratio of volume of liquid region to the whole domain).

2. Analytical solution for the non-Ohmic model

In the liquid phase, analytical solutions of electric field and charge density distributions are expressed as

$$E_l = a(y + b)^{1/2}, \quad q_l = \frac{a}{2C(y + b)^{1/2}}. \tag{B3}$$

In the solid phase, analytical solutions are given as

$$E_s = c(y + d)^{1/2}, \quad q_s = \frac{c}{2C\varepsilon_r(y + d)^{1/2}}, \tag{B4}$$

where the constants a, b, c, d can be obtained by solving the following coupled algebraic equations:

$$a = 2Cb^{1/2},$$
$$c = 2C\sqrt{K_r\varepsilon_r}b^{1/2},$$
$$d = (f_l + b)\frac{\varepsilon_r}{K_r} - f_l,$$
$$\frac{2}{3}a[(f_l + b)^{3/2} - b^{3/2}] + \frac{2}{3}c[(1 + d)^{3/2} - (f_l + d)^{3/2}] - 1 = 0.$$

It can be seen from the above equations that the hydrostatic solution of the non-Ohmic solid depends on the injection strength C, the ratios of permittivity and mobility ε_r and K_r, and the interface position f_l.

[1] A. Castellanos, *Electrohydrodynamics*, Vol. 380 (Springer, New York, 1998).
[2] F. M. J. McCluskey, P. Atten, and A. T. Perez, Heat transfer enhancement by electroconvection resulting from an injected space charge between parallel plates, Int. J. Heat Mass Transfer **34**, 2237 (1991).
[3] J. Seyed-Yagoobi, Electrohydrodynamic pumping of dielectric liquids, J. Electrostat. **63**, 861 (2005).
[4] M. Jalaal, B. Khorshidi, and E. Esmaeilzadeh, Electrohydrodynamic (EHD) mixing of two miscible dielectric liquids, Chem. Eng. J. **219**, 118 (2013).

[5] C. Louste, Z. Yan, P. Traoré, and R. Sosa, Electroconvective flow induced by dielectric barrier injection in silicone oil, J. Electrostat. **71**, 504 (2013).
[6] A. Jaworek, A. Marchewicz, A. T. Sobczyk, A. Krupa, and T. Czech, Two-stage electrostatic precipitators for the reduction of PM2.5 particle emission, Prog. Energy Combust. Sci. **67**, 206 (2018).
[7] D. Testi, Heat transfer enhancement by an impinging ionic jet in a viscous transformer coolant, Int. Commun. Heat Mass Transfer **91**, 256 (2018).
[8] P. Atten and J. C. Lacroix, Electrohydrodynamic stability of liquids subjected to unipolar injection: Non linear phenomena, J. Electrostat. **5**, 439 (1978).
[9] M. Zhang, F. Martinelli, J. Wu, P. J. Schmid, and M. Quadrio, Modal and non-modal stability analysis of electrohydrodynamic flow with and without cross-flow, J. Fluid Mech. **770**, 319 (2015).
[10] E. A. Demekhin, G. S. Ganchenko, and E. N. Kalaydin, Transition to electrokinetic instability near imperfect charge-selective membranes, Phys. Fluids **30**, 082006 (2018).
[11] P. Atten, F. McCluskey, and A. Perez, Electroconvection and its effect on heat transfer, IEEE Trans. Electr. Insul. **23**, 659 (1988).
[12] Y. Guan, R. S. Vaddi, A. Aliseda, and I. Novosselov, Experimental and numerical investigation of electrohydrodynamic flow in a point-to-ring corona discharge, Phys. Rev. Fluids **3**, 043701 (2018).
[13] M. Gao, L. S. Zhang, D. Zhang, and L. X. Zhang, Experimental study on the enhancement of free convection heat transfer under the action of an electric field, Exp. Therm. Fluid Sci. **104**, 9 (2019).
[14] P. H. Traoré, A. T. Pérez, D. Koulova, and H. Romat, Numerical modelling of finite-amplitude electro-thermo-convection in a dielectric liquid layer subjected to both unipolar injection and temperature gradient, J. Fluid Mech. **658**, 279 (2010).
[15] P. Traorè and A. T. Pèrez, Two-dimensional numerical analysis of electroconvection in a dielectric liquid subjected to strong unipolar injection, Phys. Fluids **24**, 037102 (2012).
[16] P. A. Vázquez and A. Castellanos, Numerical simulation of EHD flows using discontinuous Galerkin finite element methods, Comput. Fluids **84**, 270 (2013).
[17] J. Wu, P. A. Vázquez, P. Traoré, and A. T. Pérez, Finite amplitude electroconvection induced by strong unipolar injection between two coaxial cylinders, Phys. Fluids **26**, 124105 (2014).
[18] E. A. Demekhin, N. V. Nikitin, and V. S. Shelistov, Direct numerical simulation of electrokinetic instability and transition to chaotic motion, Phys. Fluids **25**, 122001 (2013).
[19] S. Rashidi, H. Bafekr, R. Masoodi, and E. M. Languri, EHD in thermal energy systems - A review of the applications, modelling, and experiments, J. Electrostat. **90**, 1 (2017).
[20] D. Nakhla, H. Sadek, and J. S. Cotton, Melting performance enhancement in latent heat storage module using solid extraction electrohydrodynamics (EHD), Int. J. Heat Mass Transfer **81**, 695 (2015).
[21] D. Nakhla, E. Thompson, B. Lacroix, and J. S. Cotton, Measurement of heat transfer enhancement in melting of n-Octadecane under gravitational and electrohydrodynamics (EHD) forces, J. Electrostat. **92**, 31 (2018).
[22] R. Chicón and A. T. Pérez, Instability of an interface between air and a low conducting liquid subjected to charge injection, Phys. Fluids **18**, 104108 (2006).
[23] R. Chicón and A. T. Pérez, The stability of a horizontal interface between air and an insulating liquid subjected to charge injection, Phys. Fluids **26**, 034103 (2014).
[24] F. Li, O. Ozen, N. Aubry, D. T. Papageorgiou, and P. G. Petropoulos, Linear stability of a two-fluid interface for electrohydrodynamic mixing in a channel, J. Fluid Mech. **583**, 347 (2007).
[25] B. Jayaraman and W. Shyy, Modeling of dielectric barrier discharge-induced fluid dynamics and heat transfer, Prog. Aerosp. Sci. **44**, 139 (2008).
[26] J. Lindström and J. Nordström, A stable and high-order accurate conjugate heat transfer problem, J. Comput. Phys. **229**, 5440 (2010).
[27] C. K. Aidun and J. R. Clausen, Lattice-Boltzmann method for complex flows, Annu. Rev. Fluid Mech. **42**, 439 (2010).
[28] Q. Li, K. H. Luo, Q. J. Kang, Y. L. He, Q. Chen, and Q. Liu, Lattice Boltzmann methods for multiphase flow and phase-change heat transfer, Prog. Energy Combust. Sci. **52**, 62 (2016).
[29] Y. Huo and Z. Rao, Lattice Boltzmann simulation for solid–liquid phase change phenomenon of phase change material under constant heat flux, Int. J. Heat Mass Transfer **86**, 197 (2015).

[30] S. Chen and G. D. Doolen, Lattice Boltzmann method for fluid flows, Annu. Rev. Fluid Mech. **30**, 329 (1998).
[31] M. Wang and Q. Kang, Modeling electrokinetic flows in microchannels using coupled lattice Boltzmann methods, J. Comput. Phys. **229**, 728 (2010).
[32] K. Luo, J. Wu, H. L. Yi, and H. P. Tan, Lattice Boltzmann model for Coulomb-driven flows in dielectric liquids, Phys. Rev. E **93**, 023309 (2016).
[33] K. Luo, J. Wu, H. L. Yi, and H. P. Tan, Lattice Boltzmann modelling of electro-thermo-convection in a planar layer of dielectric liquid subjected to unipolar injection and thermal gradient, Int. J. Heat Mass Transfer **103**, 832 (2016).
[34] K. Luo, J. Wu, H. L. Yi, and H. P. Tan, Numerical investigation of heat transfer enhancement in electro-thermo-convection in a square enclosure with an inner circular cylinder, Int. J. Heat Mass Transfer **113**, 1070 (2017).
[35] W. Hassen, L. Kolsi, H. F. Oztop, A. A. A. A. Al-Rashed, M. N. Borjini, and K. Al-Salem, Electro-thermo-capillary-convection in a square layer of dielectric liquid subjected to a strong unipolar injection, Appl. Math. Modell. **63**, 349 (2018).
[36] Y. Hu, D. Li, X. Niu, and Y. Zhang, Lattice Boltzmann model for the axisymmetric electro–thermo-convection, Comput. Math. Appl. **78**, 55 (2019).
[37] J. Wang, M. Wang, and Z. Li, A lattice Boltzmann algorithm for fluid–solid conjugate heat transfer, Int. J. Therm. Sci. **46**, 228 (2007).
[38] L. Li, C. Chen, R. Mei, and J. F. Klausner, Conjugate heat and mass transfer in the lattice Boltzmann equation method, Phys. Rev. E **89**, 043308 (2014).
[39] L. Wang, Y. Zhao, X. Yang, B. Shi, and Z. Chai, A lattice Boltzmann analysis of the conjugate natural convection in a square enclosure with a circular cylinder, Appl. Math. Modell. **71**, 31 (2019).
[40] P. Atten, Electrohydrodynamic instability and motion induced by injected space charge in insulating liquids, IEEE Trans. Dielectr. Electr. Insul. **3**, 1 (1996).
[41] A. T. Pérez and A. Castellanos, Role of charge diffusion in finite-amplitude electroconvection, Phys. Rev. A **40**, 5844 (1989).
[42] K. Luo, J. Wu, H. L. Yi, L. H. Liu, and H. P. Tan, Hexagonal convection patterns and their evolutionary scenarios in electroconvection induced by a strong unipolar injection, Phys. Rev. Fluids **3**, 053702 (2018).
[43] Z. Chai and B. Shi, A novel lattice Boltzmann model for the Poisson equation, Appl. Math. Model. **32**, 2050 (2008).
[44] X. He and L. S. Luo, Theory of the lattice Boltzmann method: From the Boltzmann equation to the lattice Boltzmann equation, Phys. Rev. E **56**, 6811 (1997).
[45] M. Zhang, Weakly nonlinear stability analysis of subcritical electrohydrodynamic flow subject to strong unipolar injection, J. Fluid Mech. **792**, 328 (2016).
[46] R. Chicón, A. Castellanos, and E. Martin, Numerical modelling of Coulomb-driven convection in insulating liquids, J. Fluid Mech. **344**, 43 (1997).
[47] K. Luo, J. Wu, H. L. Yi, and H. P. Tan, Three-dimensional finite amplitude electroconvection in dielectric liquids, Phys. Fluids **30**, 023602 (2018).
[48] J. Wu, P. Traoré, P. A. Vázquez, and A. T. Pérez, Onset of convection in a finite two-dimensional container due to unipolar injection of ions, Phys. Rev. E **88**, 053018 (2013).
[49] J. Wu, P. Traore, C. Louste, L. Dascalescu, F.-B. Tian, and A. T. Perez, Effect of the mobility parameter on the oscillatory electroconvection of dielectric liquids subject to strong unipolar charge injection, IEEE Trans. Ind. Appl. **50**, 2306 (2014).
[50] T. Zhang, B. Shi, Z. Guo, Z. Chai, and J. Lu, General bounce-back scheme for concentration boundary condition in the lattice-Boltzmann method, Phys. Rev. E **85**, 016701 (2012).
[51] Z. Guo, C. Zheng, and B. Shi, An extrapolation method for boundary conditions in lattice Boltzmann method, Phys. Fluids **14**, 2007 (2002).
[52] F. Vega and A. T. Pérez, Instability in a non-ohmic/ohmic fluid interface under a perpendicular electric field and unipolar injection, Phys. Fluids **14**, 2738 (2002).